Acta Biomaterialia 6 (2010) 4657–4665

Contents lists available at ScienceDirect

Acta Biomaterialia

journal homepage: www.elsevier.com/locate/actabiomat

Predicting bulk mechanical properties of cellularized collagen gels using multiphoton microscopy

C.B. Raub [a], A.J. Putnam [a,b], B.J. Tromberg [c,d], S.C. George [a,b,*]

[a] Department of Biomedical Engineering, University of California, Irvine, CA 92697, USA
[b] Department of Chemical Engineering and Materials Science, University of California, Irvine, CA 92697, USA
[c] Department of Surgery, University of California, Irvine, CA 92697, USA
[d] The Beckman Laser Institute and Medical Clinic, University of California, Irvine, CA 92697, USA

ARTICLE INFO

Article history:
Received 11 March 2010
Received in revised form 15 June 2010
Accepted 1 July 2010
Available online 8 July 2010

Keywords:
Collagen
Fibroblast
Second harmonic
Fluorescence
Mechanical properties

ABSTRACT

Cellularized collagen gels are a common model in tissue engineering, but the relationship between the microstructure and bulk mechanical properties is only partially understood. Multiphoton microscopy (MPM) is an ideal non-invasive tool for examining collagen microstructure, cellularity and crosslink content in these gels. In order to identify robust image parameters that characterize microstructural determinants of the bulk elastic modulus, we performed serial MPM and mechanical tests on acellular and cellularized (normal human lung fibroblasts) collagen hydrogels, before and after glutaraldehyde crosslinking. Following gel contraction over 16 days, cellularized collagen gel content approached that of native connective tissues (~200 mg ml^{-1}). Young's modulus (E) measurements from acellular collagen gels (range 0.5–12 kPa) exhibited a power-law concentration dependence (range 3–9 mg ml^{-1}) with exponents from 2.1 to 2.2, similar to other semiflexible biopolymer networks such as fibrin and actin. In contrast, cellularized collagen gel stiffness (range 0.5–27 kPa) produced concentration-dependent exponents of 0.7 uncrosslinked and 1.1 crosslinked (range ~5–200 mg ml^{-1}). The variation in E of cellularized collagen hydrogels can be explained by a power-law dependence on robust image parameters: either the second harmonic generation (SHG) and two-photon fluorescence (TPF) (matrix component) skewness (R^2 = 0.75, exponents of -1.0 and -0.6, respectively); or alternatively the SHG and TPF (matrix component) speckle contrast (R^2 = 0.83, exponents of −0.7 and −1.8, respectively). Image parameters based on the cellular component of TPF signal did not improve the fits. The concentration dependence of E suggests enhanced stress relaxation in cellularized vs. acellular gels. SHG and TPF image skewness and speckle contrast from cellularized collagen gels can predict E by capturing mechanically relevant information on collagen fiber, cell and crosslink density.

1. Introduction

Type I collagen is an important stress-bearing component of extracellular matrix and connective tissue. The organization and crosslinking of collagen monomers, fibrils, fibers and fiber networks may largely determine bulk mechanical properties of collagen-rich connective tissues. The mechanical properties of the extracellular matrix profoundly influence cell behavior, including proliferation [1], morphology [2], migration [3] and differentiation [4]. Conversely, cells can influence their micromechanical environment through matrix deposition [5], degradation [6] and crosslinking [7]. This dynamic interaction between cells and matrix plays an important, but only partially understood, role in wound healing, fibrosis, tumor growth, cancer metastasis and atherosclerosis.

Previous research efforts have sought to understand and control the dynamic interactions between collagen and cells in order to manipulate cell behavior and develop tissue-engineered constructs in vitro with mechanical properties similar to those of healthy native tissue. The fibroblast-seeded collagen gel has served as a useful model to assess fibroblast response to biomechanical and biochemical stimuli [8–11]. A particularly important feature is the ability of the fibroblast to contract collagen gels, and thus concentrate collagen to levels typically found in vivo (>100 mg ml^{-1}) [12]. Multiphoton microscopy (MPM) can image cellularized collagen gels using endogenous second-harmonic generation (SHG) and two-photon fluorescence (TPF) to provide unique information about collagen content and microstructure [13], and endogenous intracellular and matrix crosslink fluorophores, respectively [14]. We have previously assessed collagen microstructure using SHG signal imaging and demonstrated the potential to characterize bulk

* Corresponding author. Address: Department of Biomedical Engineering, 2420 Engineering Hall, University of California, Irvine, CA 92697-2730, USA. Tel.: +1 949 824 3941; fax: +1 949 824 2541.
E-mail address: scgeorge@uci.edu (S.C. George).

1742-7061/$ - see front matter © 2010 Acta Materialia Inc. Published by Elsevier Ltd. All rights reserved.
doi:10.1016/j.actbio.2010.07.004

mechanical properties in both acellular gels (4 mg ml^{-1} collagen content) [15,16] and native tissue (tracheal mucosa of the rabbit) [17]. The bulk stiffness of cellularized gels is likely to be affected by the collagen microstructure, cell activity and the presence of crosslinks in the extracellular matrix. It is hypothesized that robust image parameters may be derived from SHG and TPF signals which directly relate to these determinants of cellularized gel mechanics.

The objectives of this study were twofold: (i) to determine the concentration-dependent Young's moduli of cellularized gels over a range spanning in vivo (10–200 mg ml^{-1}) collagen concentrations; and (ii) to determine if MPM image parameters can predict Young's modulus. We found power-law dependences for the Young's modulus on collagen concentration, with a smaller power for cellularized gels (relative to acellular). The skewness and speckle contrast of SHG signal and TPF signal relate to collagen concentration by an inverse power-law, corroborated by simulated images of the SHG signal possessing a similar signal pattern (e.g. with the appearance of a random fiber network). The Young's moduli of cellularized gels correlates with the SHG and TPF skewness and speckle contrast in a power-law relationship, determined by multiple linear regression on log-transformed data. Our results suggest that cellularized gels exhibit significant stress relaxation, and that MPM can be used to predict bulk mechanical properties of cellularized collagen gels non-invasively over a wide range of collagen concentrations, including those found in vivo.

2. Materials and methods

2.1. Acellular collagen hydrogels

Acellular collagen hydrogels were prepared as previously described at pH 6.5, creating coarse-structured gels with large fiber diameters and large pores [16]. Final gel preparations contained 0.9 ml of 3–9 mg ml^{-1} collagen, and were allowed to polymerize at room temperature for 24 h before mechanical testing and imaging. For mechanical (indentation) testing, the samples remained in the original polymerization chambers (12-well glass-bottomed plate, MatTek Corporation, Ashland, MA) thus avoiding irreversible gel deformation. After glutaraldehyde (GTA) crosslinking (room temperature, 4% GTA/PBS, 24 h) and extensive rinses with PBS to remove unreacted GTA, the gels were again tested via indentation.

2.2. Cellularized collagen gels

Cellularized collagen gels were prepared similarly to acellular gels, except after all other components were mixed on ice and pH was adjusted to 6.5 with a small amount of sodium hydroxide, 50,000 normal human lung fibroblasts (NHLFs, passages 3–7, Lonza, Basel, Switzerland) were added per milliliter of a 4 mg ml^{-1} collagen solution. The NHLFs had undergone monolayer culture to 70–80% confluency under standard tissue culture conditions as previously described [18]. About 0.5 ml of the collagen–NHLF solution was pipetted into wells of two 24-well plates (Corning) and allowed to polymerize at room temperature (24 °C) for 1 h, creating 16 tissue constructs. After 1 h, excess Dulbecco's Modified Eagle's Medium (DMEM) was added and changed several times during the first day of culture to ensure equilibration to pH 7.4. The constructs were cultured in DMEM overnight, and then released from the wells using a sterile spatula, placed in 13.5 cm diameter Petri dishes, and covered with DMEM supplemented with 10% fetal bovine serum (FBS, Sigma, St. Louis, MO). These floating gels were cultured in standard conditions for 16 days, during which time gels were periodically removed from the Petri dishes using a spoon-shaped sterile spatula for imaging and mechanical testing.

In a second experiment, cellularized gels were prepared identically except the polymerization occurred at pH 9.5, which produces a collagen network with more, smaller diameter fibers [16]. These gels were cultured for 12 days in identical conditions, except for some gels DMEM media plus 10% FBS was supplemented with additional soluble factors: 2 ng ml^{-1} TGF-β2, 35 pg ml^{-1} PGE2 or 10 μM GM6001. TGF-β2 has been shown to affect alpha-smooth muscle actin [19] and tenascin expression, as well as SHG signal from a lung fibroblast-seeded collagen gel construct [8], and has been shown to enhance lung fibroblast proliferation and matrix synthesis [20]. In contrast, PGE2 has negative effects on lung fibroblast proliferation and matrix synthesis [21–23]. GM6001 is an inhibitor of MMP-1, -2, -3, -8 and -9, and is known to inhibit lung fibroblast-mediated collagen gel contraction [24].

In a third experiment, cellularized gels were prepared identically to the time-course experiment except that some gels were polymerized with 25 μg ml^{-1} DQ collagen (type I from bovine skin, fluorescein conjugate, Invitrogen, Carlsbad, CA). After 1 week of floating culture, as described above, the gels were imaged with a confocal fluorescence feature of the Zeiss LSM 510Meta, with excitation wavelength of 488 nm and emission filter of 500–550 nm.

GTA crosslinking of some of the cellularized gels occurred after initial imaging and mechanical testing. Gels were incubated at room temperature in 4% GTA/PBS for 24 h, and then washed for several hours with 3–5 × 50 ml PBS. Estimated collagen concentration (c, mg ml^{-1}) was calculated by dividing initial collagen mass in the gels (2 mg) by gel volume calculated from caliper measurements of gel height (h, mm), and diameter (d, mm), according to the following relation: $c = 2/\left(\frac{\pi d^2 h}{4}\right)/1000$.

2.3. Multiphoton microscopy

A LSM 510 Meta multiphoton microscope (Zeiss, Jena, Germany) was used for all imaging experiments. All SHG and TPF signals were collected in the epi-configuration with an Achroplan 40×/0.8 NA water-immersion objective (Zeiss). Each 12-bit image contained 512 × 512 pixels, and each pixel was ~440 × 440 nm. Pixel sampling rate was 625 kHz; pixel dwell time was 1.6 μs. Cellularized collagen gels were placed on 22 × 50 mm No. 1 coverslips (170 μm thickness) for imaging. Multiphoton signals were produced by a circularly polarized Chameleon laser tuned to 780 nm. Power before the objective was ~102 mW, and at the sample focus ~92 mW. The SHG signal was collected using the instrument's Meta detector, with wavelength cutoff points set at 383 and 405 nm, whereas the TPF signal was collected with an infrared-blocking 500–550 nm bandpass filter. At this excitation (780 nm), TPF emission at 500–550 is restricted mainly to: GTA [15] and pyridinium-type crosslinks [25,26] in collagen; and NADH, FAD, riboflavin and other vitamin-derived fluorophores in cells [27,28], whereas the SHG signal is specific for collagen. SHG images, signal averaged over 16 frames, were collected within the first 10 μm from the tissue surface in the region of highest SHG signal (before depth-dependent decay) to provide the best assessment of collagen microstructure. Five single-image frames were collected per tissue (with a lateral separation of 1.1 mm).

2.4. Image analysis

All image analysis was performed with ImageJ (Wayne Rasband, NIH, Bethesda, MD). Noise-subtraction was performed on all images in the following manner: 5–10 void regions from 5 to 10 SHG and TPF images were traced and the mean and standard deviation of pixel intensities were quantified, and found to be consistent among the image sets. The noise threshold was set at the mean plus three times the standard deviation from these void regions. SHG and TPF images were smoothed, and TPF images were

further despeckled (since they contained a higher noise floor than SHG images) using the corresponding ImageJ processing tools.

Matrix- and cell-derived TPF signal from images of uncrosslinked and GTA-crosslinked cellularized gels were separated by using a mask defined by a threshold. The threshold was easily determined, as the cell and matrix contributions to the TPF signal were disparate. In uncrosslinked gels, the image mean intensity was used as the threshold separating cell-derived signal (brighter than mean) and matrix-derived signal (less intense than the mean). In GTA-crosslinked gels, the mask threshold was visually determined, at a level providing clear separation between cell-associated (brighter) and matrix-associated (less intense) TPF signals. Masked pixels were assigned values of zero, while unmasked pixels retained their values.

The mean signal intensity, signal image area fraction, and skewness of the pixel histogram were calculated in ImageJ. Skewness is defined by the computational formula:

$$skew = \left\{ n\sum X_i^3 - 3\sum X_i \sum X_i^2 + \frac{2(\sum (X_i)^3)}{n} \right\} \Big/ \{(n-1)(n-2)s^3\}, \quad (1)$$

in which n is the number of pixels, X_i the intensity of pixel i, and s is the standard deviation. In practical terms, skewness describes the symmetry of the pixel histogram. A right-weighted (toward more intense signal) pixel distribution produces a positive skew, whereas a left-weighted pixel distribution produces a negative skew. An equally weighted Gaussian distribution has a skewness of zero. To show the effects on skewness of images with sparse and dense SHG and TPF signal patterns, representative images, pixel histograms and skewness values are shown (see Supplementary Data, Fig. S1).

The speckle contrast was calculated using a Matlab (version 7.4.0, Natick, MA) routine in which the speckle contrast value of each central pixel was the standard deviation divided by the mean of the pixel region. A pixel region of 2401 (49×49 pixels or 1055 μm^2) was empirically determined to produce optimal variation in the speckle contrast parameter. The mean speckle contrast of each image was calculated from the pixel values.

2.5. SHG image texture simulation

The textural features of SHG images from collagen gels were simulated using a Matlab routine. The constructed images were meant to simulate images of a randomly oriented collagen fiber network, in order to determine the relationship between robust, gain-independent image parameters and fiber number density. Collagen fiber segments within the MPM image plane were simulated as two-dimensional elliptical Gaussian functions. The length and width of the fiber segments were distributed normally, with mean and standard deviation determined from $n = 50$ line-segment measurements from SHG images of real collagen gels. Gaussian peak intensity was directly related to the length and width, so that larger fiber segments possessed proportionally more intense signals. Furthermore, the fiber edges were defined where the signal fell to $1/e^2$ times the maximum intensity of each Gaussian function. The simulated fiber areas and intensities were determined so that SHG images from cellularized gels at day 0 of culture would have similar mean intensity and signal area fraction to the simulated image of corresponding fiber number density. Fiber orientations were distributed uniformly through 360°, and positioned at random locations within a 512×512 pixel matrix. Intersecting fibers were allowed to superimpose, creating a linear relationship between mean image intensity and fiber number density, as well as a reasonable approximation to the texture of SHG images from cellularized gels containing 4–200 mg ml^{-1} collagen.

In order to relate simulated images to SHG images from cellularized gels, simulated images were assigned collagen concentrations equal to the number of Gaussian "fibers" in the simulation times a scaling factor, with units of mg ml^{-1} $fiber^{-1}$. The scaling factor was determined by counting the number of fiber segments in SHG images of cellularized gels at day 0 of culture. These SHG images were thresholded at the noise-cutoff, despeckled as before to remove remaining noise, and a binary opening algorithm was performed in ImageJ to isolate adjacent fibers. Then, particle analysis was performed in ImageJ to count particles larger than 1 μm^2. It was determined that the day 0 gel images contained 178 ± 34 fibers (mean ± SD), with an average gel concentration of 6.4 mg ml^{-1}. Therefore the scaling factor used for simulated images containing 200–5000 fiber segments was 0.0356 mg ml^{-1} $fiber^{-1}$. A second scaling factor was used to ensure the brightness of individual Gaussian ellipses was similar to the collagen fiber SHG signal, and that the overall simulated image intensity was roughly equal to that from SHG images of day 0 cellularized gels.

2.6. Mechanical testing

After multiphoton imaging, NHLF-seeded collagen hydrogels were mechanically tested using a Synergie 100 testing system (MTS Systems Corporation, Eden Prarie, MN). The hydrogels were placed on a 50 mm diameter platen covered with 600-grade ultrafine waterproof sandpaper (3 M), attached using double-sided tape, to prevent slipping. Before testing, gel height, h, and diameter, d, were measured using a caliper, and found to be in the range of 1–2 mm (h) and 4–16 mm (d). Each gel was compressed to 10% of the gel height with specially constructed 0.65 mm radius (a), non-porous, cylindrical aluminum platens. Indentation occurred at a rate of 0.05 mm s^{-1} and the resulting force was measured using a 10 N load cell, while strain was recorded based on motion of the actuator, and defined as percentage of the original sample height. Due to the small ratio of a/h, stresses beneath the platen are assumed to be non-uniform, with compressive stresses at the platen center but tensile stresses at the edges, as previously described [29]. All E were calculated assuming the gels behave as thin elastic layers bonded to a rigid bottom surface [29], directly related to the ratio a/h and the linear slope of the low strain stress–strain curve. Cellularized gels typically displayed linear stress–strain relationships through 10% strain (see Supplementary Data, Fig. S2).

Rheology was performed on GTA-crosslinked acellular gels (diameter 16 mm) only using an AR-G2 rheometer (TA Instruments, New Castle, DE) with a 20 mm diameter parallel plate configuration and a 0.7 mm gap. The gels were compressed slightly (0.1 N), and tested at an oscillation frequency of 0.01 (frequency independent), to confirm linearity of E measurements correlated vs. G' (slope $m = 2.25$, $R^2 = 0.90$, Supplementary Data, Fig. S2). This correlation is consistent with linear elasticity theory. The ratio of $E/G' = 2.25$ corresponds to a Poisson ratio of ~0.13 which is consistent with previous reports in acellular collagen gels [30]. Uncrosslinked gels could not be tested serially in indentation and shear due to gel fragility during transportation between testing devices.

2.7. Sircol assay

After imaging and mechanical testing, the collagen content of cellularized gels was assessed using the Sircol assay (Accurate Chemical and Scientific Corporation, Westbury, NY) following a manufacturer-defined protocol for assessing pepsin-soluble collagen. Collagen gels were mixed with 5 mg ml^{-1} pepsin from porcine stomach mucosa (Sigma) dissolved in 0.5 M acetic acid, and digested for 24 h at 4 °C.

2.8. Statistics

Regressions and *t*-tests were performed in Excel (Microsoft, Redmond, WA). Multiple linear regression was performed on log-transformed data using SigmaStat (Systat Software, San Jose, CA).

3. Results

3.1. Free-floating cellularized gels contract without losing collagen content

During the 16 day course of free-floating culture, the fibroblast-embedded collagen gels contracted from 320 ± 40 μl on day 0 to 14 ± 4 μl on day 15 (Fig. 1). At polymerization, the collagen content of the gels was 2 mg (the gels were formed from 500 μl of a 4 mg ml^{-1} collagen solution), but the gel volume decreased immediately upon release of the anchored gels into free-floating culture. Despite the large decrease in gel volume during the culture period, the amount of pepsin-soluble collagen within the gels did not change significantly (160 ± 60 μg on day 0 to 150 ± 40 μg on day 15; *t*-test, $P = 0.46$). Assuming that the collagen content of the gels remained constant, the estimated collagen concentration in the gels can be shown to increase, from 6 ± 1 mg ml^{-1} on day 1 to 160 ± 50 mg ml^{-1} on day 15 (Fig. 1). These data indicate that the free-floating cellularized gels tested span a range of collagen concentrations that include sparse and dense connective tissues.

3.2. Multiphoton images reveal changes in microstructure and cellularity during contraction

In order to understand the microstructure–mechanics relationships of cellularized gels during cell-mediated matrix contraction, collagen structure was assessed from SHG images, while cellularity was assessed from TPF images. SHG (Fig. 2A–C) and TPF (Fig. 2D–F) images from gels show clear increases in fiber number density and cellularity, respectively, during gel contraction. Textural simulations of SHG images using a randomly oriented collagen network (Fig. 2G–I) contain normally distributed fiber diameters (3.7 ± 2.1 μm) and lengths (23.6 ± 8.2 μm) based on measurements from 50 fibers. The simulations have a similar appearance to the SHG images of cellularized gels. The Gaussian signal intensity profiles of simulated fibers fit closely the SHG intensity profiles from real collagen fiber segments (see Supplementary Data, Fig. S3). Particle analysis of SHG images of cellularized gels on day 0 of culture revealed 178 ± 34 fiber segments (mean ± SD). Based on this measurement, simulation images containing 200–5000 fiber segments were assigned concentration values of 7–180 mg ml^{-1}. Visual comparison of SHG images and simulations shows a rough parity of texture and collagen fiber density for similar collagen concentrations (Fig. 2A–C vs. Fig. 2G–I).

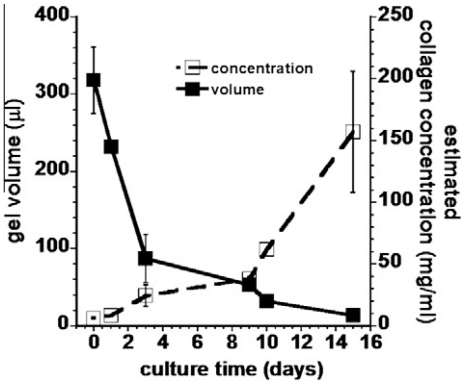

Fig. 1. Gel volume (□) and estimated concentration (□) for $n = 16$ cellularized gels collected during 16 days of floating culture.

Besides fiber morphology and number density, structural characteristics that may affect bulk mechanics were immediately apparent from SHG and TPF images. Cells exclude the collagen network creating void regions in the matrix (Fig. 2C, arrow), and collagen fibers are packed to greater density with smaller pores as the gels contract (Fig. 2C, arrowhead).

3.3. Multiphoton image parameters correlate with collagen content

Several signal and image parameters changed during the 16 day in vitro culture period. Trends from the textural simulations suggest that the functional form of SHG image parameters is largely due to changes in collagen fiber concentrations (Fig. 3A,C,E,G, SHG vs. simulation). For example, SHG signal intensity is a linear function of collagen concentration (Fig. 3A, solid line, $m = 6.8$ a.u. mg^{-1} ml^{-1}, $R^2 = 0.78$), which is corroborated by the linear relationship between image intensity and concentration in the simulated images (Fig. 3B, dashed line, $m = 6.9$ a.u. mg^{-1} ml^{-1}, $R^2 = 1.0$). In contrast, matrix TPF image fraction also increases linearly with collagen concentration but the slope is ~7-fold greater for GTA-crosslinked gels ($R^2 = 0.95$) than for uncrosslinked gels ($R^2 = 0.84$). The cell-derived TPF signal increases with collagen concentration, but with a weaker linear relationship (Fig. 3B, open circles, $R^2 = 0.53$).

SHG signal area fraction increases quickly to a plateau near 100% by ~60 mg ml^{-1} (Fig. 3C, solid markers), and depends upon collagen concentration in a logarithmic fashion ($R^2 = 0.66$ for the linear fit of ln(1 – area fraction) vs. concentration). This relationship is confirmed by the simulated signal area fraction (Fig. 3C, open markers), which reaches a plateau near 100% by ~100 mg ml^{-1} ($R^2 = 0.99$ for the linear fit of ln(1 – area fraction) vs. concentration). The matrix-derived TPF signal from GTA-crosslinked gels occupies nearly the entire image area (Fig. 3D, filled diamonds), and the matrix-derived TPF signal image fraction from uncrosslinked gels increases in logarithmic form (Fig. 3D, open diamonds). In contrast, the cell-derived TPF signal area fraction increases linearly with collagen concentration (Fig. 3D, open circles).

The signal intensity is gain-dependent and the area fraction possesses a limited range, decreasing the utility of these parameters for robust characterization of mechanically important microstructural features of cellularized gels. However, image parameters such as skewness and speckle contrast are gain-independent and are thus more robust parameters for potentially characterizing structural features that impact bulk mechanics. In contrast to the linear intensity and log area fraction dependences, we find that the skewness of the image pixel histograms relates to collagen concentration in SHG images (Fig. 3E) and TPF images (Fig. 3F) with a power-law dependence (SHG, exponent $n = -0.6$, $R^2 = 0.90$; simulation, $n = -0.5$, $R^2 = 0.99$; matrix + GTA TPF, exponent $n = -0.8$, $R^2 = 0.90$; matrix TPF, exponent $n = -0.4$, $R^2 = 0.47$; cell TPF, exponent $n = -0.5$, $R^2 = 0.70$). The speckle contrast of SHG images (Fig. 3G, solid markers) and texture simulation images (Fig. 3G, open markers) scale similarly to skewness (exponent $n = -0.6$, $R^2 = 0.90$ for SHG; $n = -1.0$, $R^2 = 0.91$ for the simulation). The speckle contrast of matrix-derived TPF signals similarly decreases with increased matrix density (Fig. 3H, matrix + GTA TPF, $n = -0.3$, $R^2 = 0.93$, filled diamonds; matrix TPF, $n = -0.2$, $R^2 = 0.51$, open diamonds). In contrast, the speckle contrast of cell-derived TPF signal increases linearly with collagen concentration (Fig. 3H, $R^2 = 0.89$, open circles).

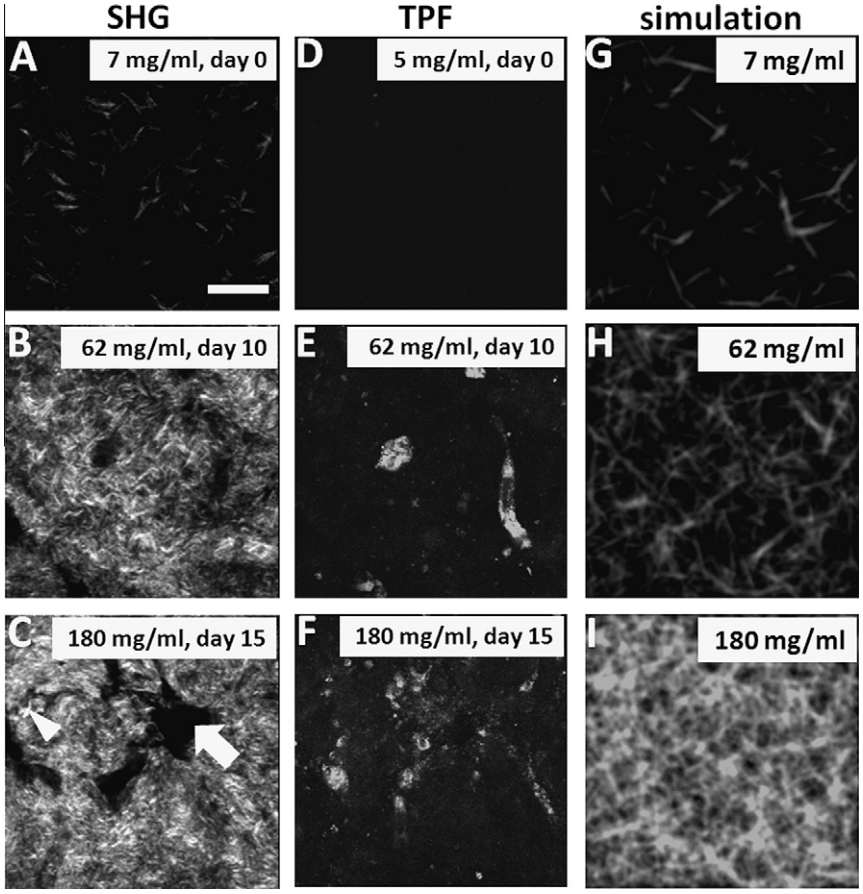

Fig. 2. Images of SHG signal (A–C), TPF signal (D–F) from cellularized gels, and simulated signal from a randomly oriented fiber network of similar texture to the SHG images (G–I). The SHG and TPF images are from cellularized gels at three stages of contraction during floating culture, and the simulated images are of roughly corresponding collagen fiber density. Estimated collagen concentration for each gel/image is indicated, and the days of culture. Bar represents 50 μm.

3.4. E depends upon collagen crosslinking, concentration and fibroblast activity

The power-law dependence of the elastic modulus on collagen concentration has been demonstrated for crosslinked and uncrosslinked acellular collagen gels containing less than 10 mg ml^{-1} collagen content [31–34], but not for cellularized gels beyond 10 mg ml^{-1}. *E* from free-floating, contracting cellularized gels was compared to that of acellular collagen gels between 3 and 9 mg ml^{-1}, before and after GTA crosslinking of the collagen network.

The concentration dependence of *E* measured from uncrosslinked and GTA-crosslinked acellular and cellularized gels is positive in all cases studied (Fig. 4A). Crosslinked gels (Fig. 4, open markers) showed increased *E* at every collagen concentration compared to uncrosslinked gels (Fig. 4, filled markers). Interestingly, acellular gels were stiffer on average at 7.5 and 9 mg ml^{-1} than cellularized gels at similar concentrations. A power-law concentration dependence of *E* produced an exponent of 2.1 uncrosslinked acellular gels (R^2 = 0.89), and 2.2 for crosslinked acellular gels (R^2 = 0.97). In contrast, the exponents for cellularized gels were smaller: ~0.7 for uncrosslinked gels (R^2 = 0.82), and ~1.1 for crosslinked cellularized gels (R^2 = 0.89).

In a parallel experiment, cellularized gels polymerized with and without DQ collagen were cultured for 1 week and the fluorescence signal from DQ collagen (excitation 488, emission 500–550) was imaged. While the control shows little fluorescence signal (Fig. 4B, lower panel), the cellularized gels containing DQ collagen, which has been shown to fluoresce when cleaved from collagen fibrils by MMP activity, showed an enhanced (~7-fold) fluorescence signal (Fig. 4B, upper panel).

In in vitro culture, the effects of cell activity, MMP activity and matrix secretion on bulk mechanics may depend upon culture time, cell concentration and the presence of soluble factors. Without explicitly measuring these independent factors, it is nevertheless desirable to see whether cell behavior may affect SHG and TPF image parameters. In a parallel experiment cellularized gels incubated for 12 days in the presence of TGF-β2, GM6001 and PGE2 contracted to 8 ± 1%, 76 ± 6%, and 87 ± 7% of their original volume (mean ± SD). The normalized SHG image intensity varied linearly with the normalized collagen concentration from these gels (Fig. 4C, m = 1.07, R^2 = 0.94), similarly to the linear relationship from cellularized gels cultured for 0–15 days (m = 0.84, R^2 = 0.76, derived from Fig. 3A, filled markers). The linearity of SHG image intensity with collagen concentration would be expected if there were no drastic alteration in the collagen network other than an increase in collagen fiber concentration. Additionally, the normalized *E* vs. collagen concentration of the soluble factor exposed cellularized gels possesses a similar power-law dependence as the cellularized gels collected between days 0 and 15 (soluble-factor-treated gels, Fig. 4D, m = 0.83, R^2 = 0.92; time-course gels, Fig. 4A, m = 0.73, R^2 = 0.82). It should be noted that the absolute magnitude of the SHG image intensity and *E* from the soluble-factor-treated gels was different than that from the time-course gels, owing to the higher polymerization pH conditions of the soluble-factor-treated gels.

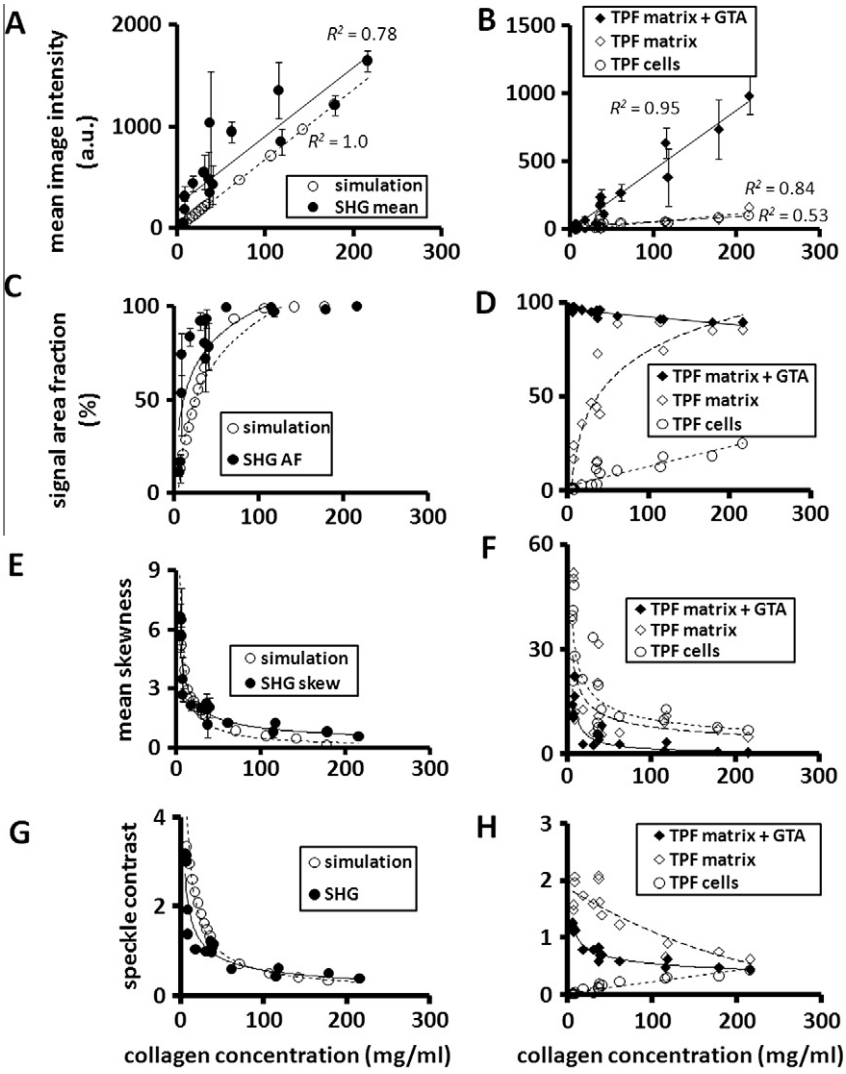

Fig. 3. Mean image intensity vs. collagen concentration for SHG and texture simulation images (A), and for TPF signal components (B). Signal image area fraction vs. collagen concentration for SHG and texture simulation images (C) and for TPF signal components (D). Mean image skewness vs. collagen concentration for SHG and texture simulation images (E) and for TPF signal components (F). Mean speckle contrast vs. collagen concentration for SHG and texture simulation images (G) and for TPF signal components (H). SHG values are filled circles; simulation values are open circles; cell-derived TPF (uncrosslinked gels) are open circles; matrix-derived TPF (uncrosslinked gels) are open diamonds); and matrix-derived TPF (crosslinked gels) are filled diamonds. Data points from SHG and TPF data represent an average of five images per gel. R^2 coefficients for the linear best fits (A, B, D), logarithmic fits (C and D) and power-law fits (E–H) are given in the text.

3.5. Skewness and speckle contrast of SHG and TPF signals predict E of cellularized gels

Multiphoton image parameters that serve as robust predictors of cellularized gel E must be gain-independent and sensitive to changes in collagen concentration, network microstructure, crosslinking and changes in cellularity. We reasoned that the skewness and speckle contrast of SHG and TPF signals may possess the desired gain-independence and structural sensitivity. To determine the strength of these image parameters in predicting E we performed multiple regression of log-transformed E values on log-transformed SHG, cell-derived TPF and matrix-derived TPF skewness (*skew*) and speckle contrast (*SC*) parameters from crosslinked and uncrosslinked cellularized gels (Fig. 5). The cell-derived TPF parameters were found to co-vary with SHG parameters, and were unable to explain the additional variation in E. We found that the relationship $E \sim skew_{SHG}^{-1.0} skew_{TPF,matrix}^{-0.6}$ provided a best fit which explained the most variation in E (Fig. 5A, $R^2 = 0.80$). Similarly, the relationship $E \sim SC_{SHG}^{-0.7} SC_{TPF,matrix}^{-1.8}$ provided a best fit which explained the most variation in E (Fig. 5B, $R^2 = 0.83$). Observation of the linear and log–log plots of the multiple regressions shows that the non-linear model using the skewness parameters tends to overestimate E of gels with sparse matrix (days 0–3, Fig. 5A, inset).

4. Discussion

Understanding the dynamic relationship between microstructure and bulk mechanics in developing engineered tissues is necessary to assess properties critical for successful development and integration upon implantation. SHG and TPF signals from cellularized collagen gels have been used to track structural changes and cellularity during tissue culture [14–16,18,35,36]. The ability of the SHG signal to distinguish collagen microstructure and the TPF signal to distinguish cross-links and cells suggests that the bulk mechanics of cellularized collagen gels may be inferred from MPM images, but few studies have attempted to correlate bulk tissue mechanics and MPM image parameters in cellularized tissues. One challenge facing the task of constructing image parameter correlations with bulk tissue properties is to identify appropriate image parameters which are sensitive to microstructural

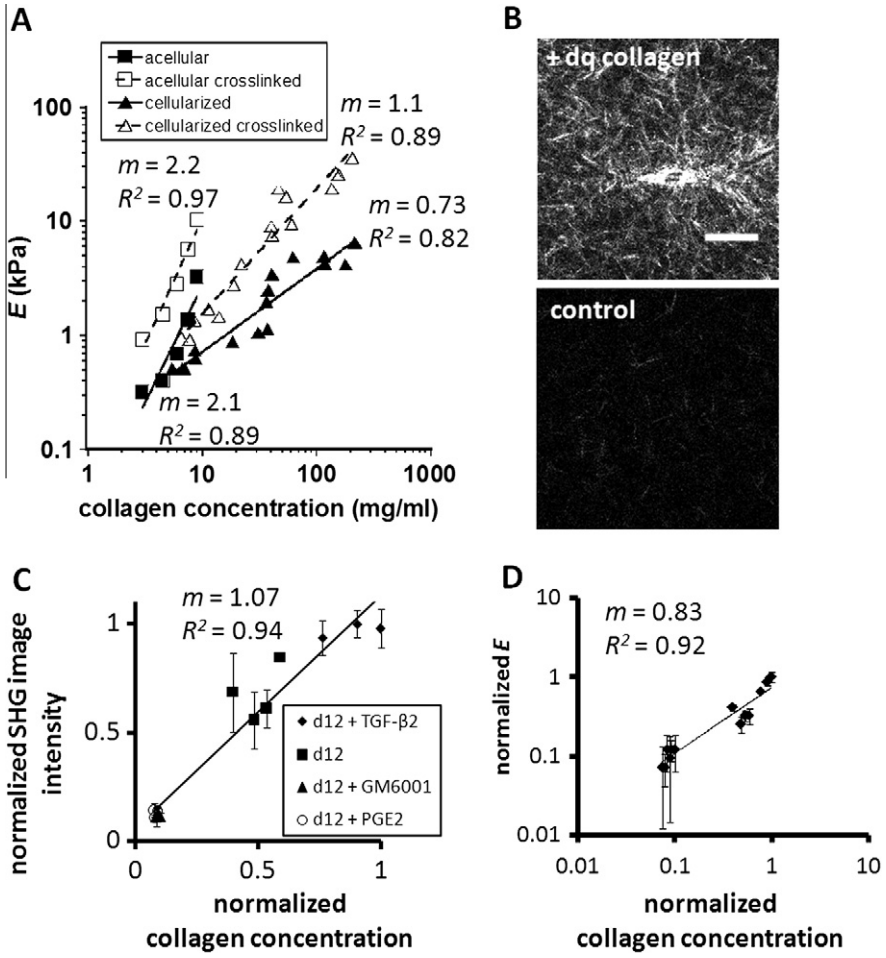

Fig. 4. (A) E measured from uncrosslinked cellularized gels (□, $n = 16$), GTA-crosslinked cellularized gels (□, $n = 16$), uncrosslinked acellular gels (□, $n = 5$), and crosslinked acellular gels (□, $n = 5$) as functions of collagen concentration. E data points represent five averaged measurements per gel. Error bars are omitted for clarity. Lines represent linear best-fits to the log-transformed data (averaged over coarse and fine-structured gels). Best-fit slopes and R^2 values are indicated next to best-fit lines. (B) Representative confocal fluorescence images of cellularized gels polymerized with DQ collagen (upper panel) and without DQ collagen (lower panel) and incubated for 7 days. Scale bar is 50 μm. (C) Normalized mean SHG image intensity vs. normalized collagen concentration for cellularized gels incubated for 12 days (d12) in DMEM + 10% FBS supplemented with 2 ng ml^{-1} TGF-β2, 35 pg ml^{-1} PGE2 or 10 μM GM6001. (D) Normalized E vs. normalized collagen concentration for the same gels, determined by indentation testing as in (A). Slopes and best-fit coefficients are indicated in the figure.

determinants of mechanics, yet independent of instrument gain and other microscope parameters. In this study we identify the SHG and TPF skewness and speckle contrast as gain-independent parameters which have predictive power for E (Fig. 5).

We also characterized a power-law dependence of E on collagen concentration with a lower power for cellularized (0.7–1.1) than acellular (2.1) gels, smaller E for uncrosslinked than crosslinked gels; and smaller E for cellularized gels than acellular gels at concentrations of 6–9 mg ml^{-1}. The power-law exponents were 2.1 and 2.2 for acellular uncrosslinked and crosslinked gels, respectively; but only 0.7 and 1.1 for cellularized uncrosslinked and crosslinked gels (Fig. 4). Our indentation testing results for acellular collagen gels are in closer agreement with a semiflexible network (exponent 1.4–2.2) [33,34,37,38], or a foam lattice theoretical scaling (exponent 2) [39,40] for networks unable to relax stress during the mechanical testing period, than with a composite model (exponent 1) [12] or rigid rod (exponent 1–2) model of the gels [41,42]. Other researchers have reported exponents of 2.1 for fibrin [32], 2.1–2.5 for actin [32,43], and 2.1–2.8 for acellular collagen gels of 0.5–5 mg ml^{-1} [31,44].

Concurrent processes of matrix synthesis, degradation and remodeling may explain the generally reduced E of cellularized gels. SHG images show evidence of matrix defects near cells (Fig. 2C); and TPF images show increasing fibroblast prevalence with culture time (Figs. 2F and 3D, open circles) which are associated with collagenase activity in collagen gels (Fig. 4B). It may not be concluded that cellularized gel E is wholly dependent on collagen concentration, despite the strong correlation of these two parameters. Time-dependent cell activity (collagenases, proliferation and collagen remodeling) might lead to a reduction in E. Yet, for the experiments described, the cell-associated TPF parameters did not improve the multiple regression of E on image parameters, which were best using SHG and matrix-derived TPF skewness and speckle contrast parameters. In addition, cellularized gels incubated for equal time (12 days) but with soluble factors known to enhance matrix remodeling (TGF-β2), inhibit matrix remodeling (PGE2) and inhibit MMPs (GM6001) were shown to possess similarly linear SHG image intensity and weak E dependencies on collagen concentration (Fig. 4C and D). Finally, Sircol assay measurements of collagen content from cellularized gels reveal minimal change in total collagen mass during 16 days of floating culture. We conclude that fibroblast-mediated matrix remodeling and enzymatic degradation may still play a role in determining cellularized tissue mechanics with the fibroblast, collagen

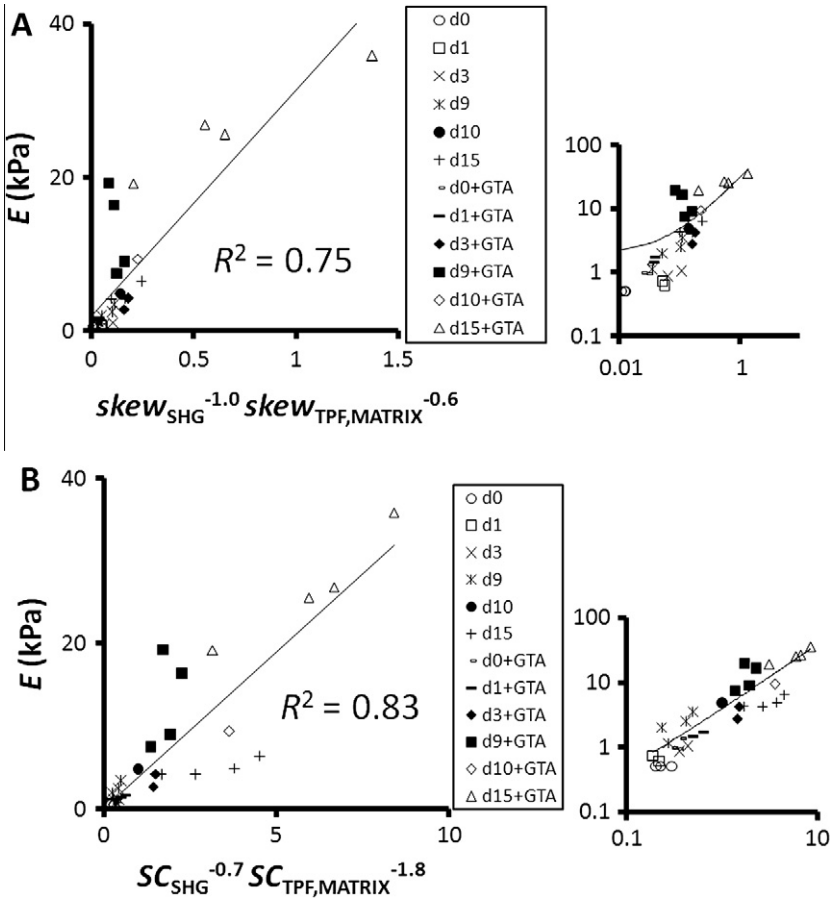

Fig. 5. (A) Non-linear best-fit model for E on SHG signal skewness and matrix-derived TPF signal skewness. Markers indicate days in culture of the collagen gels and presence of GTA crosslinking. The inset on the right is a log–log plot of the data. (B) Non-linear best-fit model for E on SHG signal speckle contrast and matrix-derived TPF signal speckle contrast. Markers indicate days (notation "d1" for day 1) in culture of the collagen gels and presence of GTA crosslinking. The inset on the right is a log–log plot of the data. Power-law best-fit exponents and R^2 values are indicated in the figure. E was averaged from five measurements per gel for $n = 16$ gels.

concentrations and soluble factors studied, but that collagen fiber density and crosslink content primarily determine the indentation mechanics of the cellularized gels.

In cellularized collagen gels, the SHG signal arises from the non-centrosymmetric, polarizable molecular structure of collagen fibrils, whereas the TPF signal originates from FAD, NADH and flavins, as well as collagen crosslinks [14,25–27,45]. Collagen second harmonic signal, cell autofluorescence and crosslink autofluorescence yield information about the distribution and structure of these tissue components. Specifically, high skewness in the image intensity histogram indicates a non-normal, right-tailed distribution of pixel intensities, consistent with mostly dim collagen fibers within the SHG and TPF images, and very few bright fibers (see Supplementary Data, Fig. S1). A low skewness indicates a symmetrical distribution, with more equal weight in left (dim fibers) and right (bright fibers) tails. As images become more populated, a more symmetrical distribution of pixel intensities is observed, reflecting the texture of a dense collagen network with unimodal morphological distribution. The speckle contrast is highest for images with high local variability, such as images of sparse cells or collagen fibers surrounded by void regions. Speckle contrast is reduced in images with less contrast, such as a uniformly filled image of a dense collagen network. Skewness and speckle contrast image parameters, while insensitive to instrument gain, are sensitive to small changes in the amount and distribution of signal-generating material, and are therefore sensitive to the same microstructural parameters of cellularized gels which determine bulk mechanics.

Finally, E has a stronger inverse correlation with SHG skewness compared to matrix-derived TPF skewness (Fig. 5A, exponent of -1.0 compared to -0.6). Conversely E is more sensitive to changes in TPF matrix-derived speckle contrast than SHG speckle contrast (Fig. 5B, exponent of -0.7 compared to -1.8). The matrix-derived TPF speckle contrast reflects the spatial organization of collagen fibers and crosslinks. Speckle contrast, as an indicator of local standard deviation, may be more sensitive to changes in signal spatial organization than skewness. It is important to note that the speckle contrast parameters provided a better fit to the cellularized gel mechanical data, although the model overestimated E from day 15 uncrosslinked gels (Fig. 5B). It is possible that cell-based matrix degradation was strongest for these cells, and that the non-linear model using SHG and matrix-derived TPF parameters is not sensitive to collagenase degradation of the collagen network. The influence of cells and crosslinks on E is also suggested by the reduced E in cellularized vs. acellular gels, and increased E in crosslinked gels (Fig. 4). These data, as well as previous studies showing a large effect of both cells [6,7] and crosslinking [7,15,46] on collagen gel stiffness, corroborate the need for robust image parameters which directly relate to structural, cellular and crosslink content patterns in cellularized gels, in order to predict gel bulk mechanics.

5. Conclusions

In summary, microstructural parameters change systematically during cell-mediated gel contraction: pores become smaller, fiber bundles become larger, and cells occupy holes in a dense

three-dimensional collagen network. Cellularized gels tend to be weaker than acellular gels at similar concentrations, and exhibit weaker concentration-dependence consistent with increased relaxation of tension within strained network elements. For cellularized collagen gels, SHG and TPF image parameters, such as skewness and speckle contrast, change with collagen fiber, crosslink and cell densities in a predictable manner. Hence, cellularized gel E can largely be predicted by variation in SHG and matrix-derived TPF speckle contrast, which depend upon collagen and crosslink spatial patterns.

Acknowledgements

We would like to thank Peter Kim and Amy VanStrien for assistance with rheological measurements, and Dr. Tatiana Krasieva for training on the multiphoton microscope and critical review of this manuscript. This work was supported, in part, by the National Heart, Lung, and Blood Institute (R01 HL067954, S.C.G.; and HL085339, A.J.P.), a Kirschstein pre-doctoral fellowship from the National Institute of Biomedical Imaging and Bioengineering (F31 EB006677, C.B.R.), and the ARCS Foundation, Orange County Chapter (Fellowship, C.B.R.). This work was made possible, in part, through access to the Laser Microbeam and Medical Program (LAMMP) at the University of California, Irvine. The LAMMP facility is supported by the National Institutes of Health under a grant from the National Center for Research Resources (NIH No. P41RR01192, B.J.T.). Support from the Arnold and Mabel Beckman Foundation is gratefully acknowledged.

Appendix A. Supplementary data

Supplementary data associated with this article can be found, in the online version, at doi:10.1016/j.actbio.2010.07.004.

References

[1] Liu M, Xu J, Souza P, Tanswell B, Tanswell AK, Post M. The effect of mechanical strain on fetal rat lung cell proliferation: comparison of two- and three-dimensional culture systems. In Vitro Cell Dev Biol Anim 1995;31:858–66.
[2] Yeung T, Georges PC, Flanagan LA, Marg B, Ortiz M, Funaki M, et al. Effects of substrate stiffness on cell morphology, cytoskeletal structure, and adhesion. Cell Motil Cytoskeleton 2005;60:24–34.
[3] Zaman MH, Trapani LM, Sieminski AL, Mackellar D, Gong H, Kamm RD, et al. Migration of tumor cells in 3D matrices is governed by matrix stiffness along with cell-matrix adhesion and proteolysis. Proc Natl Acad Sci USA 2006;103:10889–94.
[4] Engler AJ, Sen S, Sweeney HL, Discher DE. Matrix elasticity directs stem cell lineage specification. Cell 2006;126:677–89.
[5] Leung LY, Tian D, Brangwynne CP, Weitz DA, Tschumperlin DJ. A new microrheometric approach reveals individual and cooperative roles for TGF-beta1 and IL-1beta in fibroblast-mediated stiffening of collagen gels. FASEB J 2007;21:2064–73.
[6] Phillips JA, Vacanti CA, Bonassar LJ. Fibroblasts regulate contractile force independent of MMP activity in 3D-collagen. Biochem Biophys Res Commun 2003;312:725–32.
[7] Redden RA, Doolin EJ. Collagen crosslinking and cell density have distinct effects on fibroblast-mediated contraction of collagen gels. Skin Res Technol 2003;9:290–3.
[8] Thompson HG, Mih JD, Krasieva TB, Tromberg BJ, George SC. Epithelial-derived TGF-{beta}2 modulates basal and wound healing subepithelial matrix homeostasis. Am J Physiol Lung Cell Mol Physiol 2006.
[9] Grinnell F. Fibroblast–collagen-matrix contraction: growth-factor signalling and mechanical loading. Trends Cell Biol 2000;10:362–5.
[10] Arora PD, McCulloch CA. Dependence of collagen remodelling on alpha-smooth muscle actin expression by fibroblasts. J Cell Physiol 1994;159:161–75.
[11] Arora PD, Narani N, McCulloch CA. The compliance of collagen gels regulates transforming growth factor-beta induction of alpha-smooth muscle actin in fibroblasts. Am J Pathol 1999;154:871–82.
[12] Nimni ME, editor. Collagen. Boca Raton, FL: CRC Press, 1988.
[13] Williams RM, Zipfel WR, Webb WW. Interpreting second-harmonic generation images of collagen I fibrils. Biophys J 2005;88:1377–86.
[14] Zoumi A, Yeh A, Tromberg BJ. Imaging cells and extracellular matrix in vivo by using second-harmonic generation and two-photon excited fluorescence. Proc Natl Acad Sci USA 2002;99:11014–9.
[15] Raub CB, Suresh V, Krasieva T, Lyubovitsky J, Mih JD, Putnam AJ, et al. Noninvasive assessment of collagen gel microstructure and mechanics using multiphoton microscopy. Biophys J 2007;92:2212–22.
[16] Raub CB, Unruh J, Suresh V, Krasieva T, Lindmo T, Gratton E, et al. Image correlation spectroscopy of multiphoton images correlates with collagen mechanical properties. Biophys J 2008;94:2361–73.
[17] Raub CB, Mahon S, Narula N, Tromberg BJ, Brenner M, George SC. Linking optics and mechanics in an in vivo model of airway fibrosis and epithelial injury. J Biomed Opt 2010;15:015004.
[18] Thompson HG, Mih JD, Krasieva TB, Tromberg BJ, George SC. Epithelial-derived TGF-beta2 modulates basal and wound-healing subepithelial matrix homeostasis. Am J Physiol Lung Cell Mol Physiol 2006;291:L1277–1285.
[19] Wicks J, Haitchi HM, Holgate ST, Davies DE, Powell RM. Enhanced upregulation of smooth muscle related transcripts by TGF beta2 in asthmatic (myo) fibroblasts. Thorax 2006;61:313–9.
[20] Zhang S, Smartt H, Holgate ST, Roche WR. Growth factors secreted by bronchial epithelial cells control myofibroblast proliferation: an in vitro co-culture model of airway remodeling in asthma. Lab Invest 1999;79:395–405.
[21] Huang SK, White ES, Wettlaufer SH, Grifka H, Hogaboam CM, Thannickal VJ, et al. Prostaglandin E(2) induces fibroblast apoptosis by modulating multiple survival pathways. Faseb J 2009;23:4317–26.
[22] Huang SK, Wettlaufer SH, Chung J, Peters-Golden M. Prostaglandin E2 inhibits specific lung fibroblast functions via selective actions of PKA and Epac-1. Am J Respir Cell Mol Biol 2008;39:482–9.
[23] Huang S, Wettlaufer SH, Hogaboam C, Aronoff DM, Peters-Golden M. Prostaglandin E(2) inhibits collagen expression and proliferation in patient-derived normal lung fibroblasts via E prostanoid 2 receptor and cAMP signaling. Am J Physiol Lung Cell Mol Physiol 2007;292:L405–413.
[24] Mikko M, Fredriksson K, Wahlstrom J, Eriksson P, Grunewald J, Skold CM. Human T cells stimulate fibroblast-mediated degradation of extracellular matrix in vitro. Clin Exp Immunol 2008;151:317–25.
[25] Theodossiou T, Rapti GS, Hovhannisyan V, Georgiou E, Politopoulos K, Yova D. Thermally induced irreversible conformational changes in collagen probed by optical second harmonic generation and laser-induced fluorescence. Lasers Med Sci 2002;17:34–41.
[26] Kirkpatrick ND, Hoying JB, Botting SK, Weiss JA, Utzinger U. In vitro model for endogenous optical signatures of collagen. J Biomed Opt 2006;11:054021.
[27] Zipfel WR, Williams RM, Christie R, Nikitin AY, Hyman BT, Webb WW. Live tissue intrinsic emission microscopy using multiphoton-excited native fluorescence and second harmonic generation. Proc Natl Acad Sci USA 2003;100:7075–80.
[28] Georgakoudi I, Rice WL, Hronik-Tupaj M, Kaplan DL. Optical spectroscopy and imaging for the non-invasive evaluation of engineered tissues. Tissue Eng Part B Rev 2008;14:321–40.
[29] Hayes WC, Keer LM, Herrmann G, Mockros LF. A mathematical analysis for indentation tests of articular cartilage. J Biomech 1972;5:541–51.
[30] Vader D, Kabla A, Weitz D, Mahadevan L. Strain-induced alignment in collagen gels. PLoS One 2009;4:e5902.
[31] Yang YL, Kaufman LJ. Rheology and confocal reflectance microscopy as probes of mechanical properties and structure during collagen and collagen/hyaluronan self-assembly. Biophys J 2009;96:1566–85.
[32] Janmey PA, Euteneuer U, Traub P, Schliwa M. Viscoelastic properties of vimentin compared with other filamentous biopolymer networks. J Cell Biol 1991;113:155–60.
[33] Morse DC. Viscoelasticity of concentrated isotropic solutions of semiflexible polymers. 2. Linear response. Macromolecules 1998;31:7044–67.
[34] MacKintosh FC, Kas J, Janmey PA. Elasticity of semiflexible biopolymer networks. Phys Rev Lett 1995;75:4425–8.
[35] Agarwal A, Coleno ML, Wallace VP, Wu WY, Sun CH, Tromberg BJ, et al. Two-photon laser scanning microscopy of epithelial cell-modulated collagen density in engineered human lung tissue. Tissue Eng 2001;7:191–202.
[36] Kirkpatrick ND, Andreou S, Hoying JB, Utzinger U. Live imaging of collagen remodeling during angiogenesis. Am J Physiol Heart Circ Physiol 2007;292:H3198–3206.
[37] Luan Y, Lieleg O, Wagner B, Bausch AR. Micro- and macrorheological properties of isotropically cross-linked actin networks. Biophys J 2008;94:688–93.
[38] Morse DC. Viscoelasticity of concentrated isotropic solutions of semiflexible polymers. 1. Model and stress tensor. Macromolecules 1998;31:7030–43.
[39] Satcher Jr RL, Dewey Jr CF. Theoretical estimates of mechanical properties of the endothelial cell cytoskeleton. Biophys J 1996;71:109–18.
[40] Gibson LJ. Biomechanics of cellular solids. J Biomech 2005;38:377–99.
[41] Kroy K, Frey E. Force-extension relation and plateau modulus for wormlike chains. Phys Rev Lett 1996;77:306–9.
[42] Doi M, Edwards S. The theory of polymer dynamics. Oxford: Oxford University Press; 1986.
[43] Gardel ML, Shin JH, MacKintosh FC, Mahadevan L, Matsudaira P, Weitz DA. Elastic behavior of cross-linked and bundled actin networks. Science 2004;304:1301–5.
[44] Yang YL, Leone LM, Kaufman LJ. Elastic moduli of collagen gels can be predicted from two-dimensional confocal microscopy. Biophys J 2009;97:2051–60.
[45] Freund I, Deutsch M, Sprecher A. Connective tissue polarity optical second-harmonic microscopy, crossed-beam summation, and small-angle scattering in rat-tail tendon. Biophys J 1986;50:693–712.
[46] Sheu MT, Huang JC, Yeh GC, Ho HO. Characterization of collagen gel solutions and collagen matrices for cell culture. Biomaterials 2001;22:1713–9.